







Generation of broadband parabolic pulses based on a pre-chirper free, core-pumped nonlinear fiber amplifier for coherent anti-Stokes Raman imaging

KANGWEN YANG,¹  JIAMEI WU,¹ JIANPENG AO,² QIANG HAO,¹ MING YAN,^{3,4}  KUN HUANG,^{3,4}  MINBIAO JI,²  AND HEPING ZENG^{1,3,4,5,*}

¹Shanghai Key Laboratory of Modern Optical System, and Engineering Research Center of Optical Instrument and System, Ministry of Education, School of Optical Electrical and Computer Engineering, University of Shanghai for Science and Technology, Shanghai 200093, China

²State Key Laboratory of Surface Physics and Department of Physics, Human Phenome Institute, Multiscale Research Institute of Complex Systems, Academy for Engineering and Technology, Key Laboratory of Micro and Nano Photonic Structures (Ministry of Education), Fudan University, Shanghai 200433, China

³State Key Laboratory of Precision Spectroscopy, East China Normal University, Shanghai 200062, China

⁴Chongqing Institute of East China Normal University, Chongqing 401121, China

⁵Jinan Institute of Quantum Technology, Jinan 250000, China

*hpzeng@phy.ecnu.edu.cn

Abstract: We report the generation of parabolic pulses with broadband spectrum from a core-pumped Yb-doped fiber amplifier seeded by a dispersion managed fiber oscillator. The net cavity dispersion of Yb-doped oscillator was continuously changed from 0.074 to -0.170 ps², which enabled us to achieve dissipative soliton, stretched pulse and soliton mode-locking operations. Spectral evolution processes in the core-pumped nonlinear fiber amplifier seeded by various input solitons were investigated experimentally and theoretically. Our finding indicates that cavity dispersion of oscillator can be used to engineer the input pulse parameter for amplifier, thus forming a pre-chirper free fiber amplification structure. In the experiment, we obtained 410-mW parabolic pulses with spectral bandwidth up to 56 nm. In combination with a passively synchronized frequency-doubled Er-doped fiber laser, we have demonstrated coherent anti-Stokes Raman imaging. The compact dual-color fiber laser source may facilitate practical applications of nonlinear biomedical imaging beyond the laboratory environment.

© 2022 Optica Publishing Group under the terms of the [Optica Open Access Publishing Agreement](#)

1. Introduction

Coherent Raman scattering microscopy (CRS), including coherent anti-Stokes Raman scattering (CARS) and stimulate Raman scattering (SRS) has become a fundamental and indispensable tool for label-free biomedical researches [1–4]. Particularly, the single-frequency CRS microscopy utilizing dual-color narrowband picosecond laser favors fast acquisition speed, which is widely used in brain tumor analysis [5], multimodal nonlinear endomicroscopic [6] and fast cell sorting [7]. Practically, one Raman band is not enough to discriminate different molecules. Therefore, multi-color CRS imaging excited by a wavelength tunable laser source is often required for better selectivity [8,9]. To further apply this nonlinear imaging method to medical field such as clinical diagnosis or intraoperative pathology, one major obstacle is the strict operation conditions for heavy and bulky lasers [10]. To overcome this limitation, robust fiber lasers with compact size, economic cost and stable performance become promising candidates in this field. Recently, various fiber design architectures such as four-wave mixing [11–13], soliton self-frequency shift

and supercontinuum [14,15] are proposed to generate tunable narrowband picosecond pulses and show their availability in nonlinear biomedical imaging.

In order to obtain tunable picosecond pulses, one can tune the wavelength in the beginning (cavity tuning), at the terminal (after main amplifier) or in the middle (before main amplifier) of a fiber laser system utilizing master oscillator power amplifier (MOPA) scheme. Cavity tuning method using tunable fiber Bragg gratings or filters inside laser oscillator is the most straightforward way but increases the risk of losing mode-locking. Due to the high peak power of amplified ultrashort optical pulse, tuning at the terminal often requires free-space filters with high damage threshold, which hampers all-fiber integration. Therefore, a practical way is to broaden the spectrum first and then use narrowband optical filter to select the wanted spectral component as seed pulse for further amplification. Owing to the small core size of fiber and high peak power of ultrashort pulse, spectral broadening can be easily implemented by coupling ultrashort pulse into a passive or active fiber [16]. Passive fibers such as photonic crystal fiber (PCF) [17,18], high nonlinear fiber or single mode fiber (SMF) [19] have been widely used for spectral broadening. The generated spectrum can cover an octave spectral range. However, the interplay of various nonlinear effects will be detrimental to the noise performance, which is harmful for the noise sensitive applications [20].

In contrast to use passive fiber, there exist techniques based on nonlinear pulse evolution in active gain fiber to achieve broadband spectrum and low intensity noise [21,22]. These methods include direct amplification, parabolic pre-shaping amplification, and pre-chirp managed amplification (PCMA) [23], as well as recently presented amplification with gain-managed nonlinearity (GMN) [16]. Direct amplification of femtosecond seed with double-clad gain fiber produces MW-level peak power ultrashort pulses with spectral bandwidth of 50-60 nm, but its free-space coupling and gain related pulse re-compressibility complicate the design [24,25]. As for the parabolic pre-shaping method, it utilizes passive fiber to reshape seed pulse into parabolic pulse so as to accumulate linear chirp in the amplifying process, thus achieving higher energy and transform-limited de-chirped pulse. In 2017, the limits of pre-shaping for femtosecond pulse amplification were explored [26]. They introduced a simplified analytical model and generated 275-fs, 4.3- μ J pulses. Their results indicated that large compression ratio and transform-limited pulse can be obtained with narrowband seed pulses by parabolic pre-shaping. To manipulate spectral broadening process by tailing chirp of the seed, a grating based pre-chirper is often added before amplifier in PCMA. Using this scheme, amplified pulses with spectral bandwidth of 41-nm and average power of \sim 100 W can be obtained [27]. Amplification with GMN can produce pulses with spectral bandwidth beyond the gain (\sim 150 nm) by using a dynamically evolving gain spectrum [16,28]. In this scheme, the nonlinear spectral broadening is balanced by gain-shaping when amplified pulse propagates in long, highly doped fibers. Although its evolution starts from similariton, the management of nonlinearity by the gain shows a distinguished feature with broadband spectrum and compressible transform limited pulse width.

Lots of previous works have been focused on building high power nonlinear amplifiers by using of double-clad gain fiber. For biomedical imaging applications, the power of ultrashort laser pulse on the sample should be well controlled below the damage threshold [29]. Considering the optimal parameters presented in previous publications [30], a typical average power of tens of milliwatts at the sample is required to conduct nonlinear imaging. In this case, core-pumped fiber laser systems providing average power of several hundreds of milliwatts are enough to meet these requirements. Chirp of the seed pulse was one of the important parameters for manipulating temporal and spectral characteristics of amplified pulse. Research has found that a well-designed negative pre-chirp can exhibit less steep wings in amplified spectrum and thus generating transform-limited pulse with minimal pedestals. Using this method, they have obtained \sim 500 mW, 134 fs laser pulses with \sim 20 nm spectral bandwidth [31]. Recently, core-pumped Yb-doped fiber amplifier utilizing PCMA structure was reported [32], generating laser pulses

with spectral bandwidth of ~ 30 nm and average power of >300 mW [33]. In contrast to PCMA, a Yb-doped core-pumped fiber amplifier was presented without pre-chirper, producing spectral broadened laser pulses with 44-nm bandwidth and 200-mW average power [34]. Their results show that pre-chirper free design seems to output wider spectral bandwidth. However, there are few works reported about broadband parabolic pulse generation in such fiber amplifiers. The pulse evolution in pre-chirper free core-pumped nonlinear fiber amplifier for different initial pulse still remain unclear.

Here, we systematically investigate pulse evolution in a pre-chirper free core-pumped fiber amplifier seeded by dispersion managed fiber oscillator. After optimizing the net cavity dispersion of the oscillator, the amplified pulses with spectral bandwidth of 56 nm and average power of 410 mW were obtained, which is to the best of our knowledge the broadest spectrum obtained from a core-pumped single-clad fiber amplifier. We then injected one portion of the amplified pulses around 1030 nm into an Er-doped fiber oscillator for implementing a passive synchronization. Using this tunable synchronized laser pulses, CARS and second harmonic generation (SHG) imaging of mouse ear sample were demonstrated.

2. Experimental setup

The experimental setup of tunable synchronized fiber lasers for CARS imaging is shown in Fig. 1. It included the Stokes light, the Pump light and the microscope. The Stokes branch was comprised of a dispersion managed Yb-doped fiber oscillator (DM-YbFO), a core-pumped single-clad nonlinear fiber amplifier, an optical filter and cascade fiber amplifiers. The DM-YbFO had figure-of-nine arrangements and could be passively mode-locked by nonlinear amplifying loop mirror (NALM). A pair of transmission gratings of 1250 lines/mm were inserted in the linear segment of the oscillator to continuously tune the net cavity dispersion. A reflect mirror was placed on a stage for precisely control of cavity length. An optical coupler with coupling ratio of 5:5 was used to connect the linear and circular segments. The 976-nm pump light with a maximum average power of 500 mW was coupled into the cavity via a wavelength division multiplexer. The gain fiber was a piece of 1.5-m Yb-doped fiber (PM-YSF-HI-HP, Nufern). A phase shifter and a 1:9 coupler were used to start mode-locking and provide output.

Spectral broadening can be realized by the core-pumped single-clad nonlinear fiber amplifier. The gain fiber was a piece of 1.5-m Yb-doped fiber with the same type of the oscillator, which was dual-pumped by two laser diodes with the maximum total average power of 1.4 W. The amplified pulses were divided into two parts by an optical coupler with coupling ratio of 1:9. The 90% port of the coupler was connected to a tunable optical filter and cascade fiber amplifier for spectral selection and power scaling. The residual pulses from the 10% port was used for injection synchronization.

The Pump branch was comprised of an all-fiber Er-doped fiber oscillator (ErFO), fiber amplifiers and frequency doubling module. The Er-doped oscillator had the same structure as the YbFO except for the transmission gratings were replaced by a fiber Bragg grating with 1580-nm central wavelength and 0.2-nm bandwidth. Output pulses from ErFO were amplified by a two stage Er-doped fiber amplifier. The lengths of gain fiber (Er 80, OFS) in both oscillator and amplifiers were 1.5 m. A periodically poled lithium niobate (PPLN) crystal with period of 20.2 μm and length of 20 mm was used for frequency doubling of amplified pulses around 1580 nm. Detailed parameters of elements used in this branch could be found in our previous publication [19].

Passive synchronization between Stokes and Pump light was achieved by injecting master laser pulses from DM-YbFO into slave laser of ErFO via a 1580/1030 wavelength division multiplexer. We used laser pulses from 10% port of the first stage Yb-doped amplifier as injecting pulses to provide enough laser power. Once the 1030-nm pulses were injected, they initiated a pulsed modulation on the quasi-CW laser beam at ErFO. This modulation-induced pulses evolved into

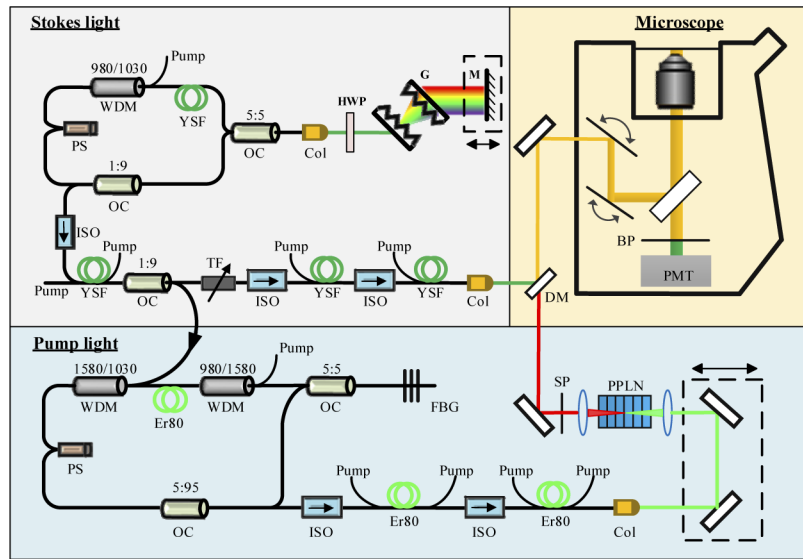


Fig. 1. Experimental setup. WDM: wavelength division multiplexer; PS: phase shifter; OC: optical coupler; HWP: half wave plate; G: grating; TF: tunable filter; ISO: isolator; SP: short pass filter; DM: dichroic mirror; BP: bandpass filter; PMT: photomultiplier tube.

stable pulses through mode-locking mechanism of the slave laser, which was NALM in our case. With continuous injection, the subsequent injected 1030-nm pulses encountered with 1580-nm pulses in the ErFO, their interaction gave rise to additional timing-dependent phase shift due to cross-phase modulation. This phase shift then forced the pulse train at 1580-nm to synchronize with the 1030-nm pulse train [35,36].

3. Experimental results and discussion

3.1. Output characteristic of the dispersion managed Yb-doped oscillator

In the following, we will discuss output characteristics with a focus on spectra in different net cavity dispersion. Stable passive mode-locking operation could be self-started, as the temporal oscilloscope trace shown in Fig. 2(a). The repetition rate of the laser oscillator was measured to be 20 MHz with a RF signal to noise ratio of >50 dB, as shown in Fig. 2(b). Laser operation for different values of net cavity dispersion can be realized by tuning the grating separation distance in the linear segment. As a result, the repetition rate changed accordingly. As shown in Fig. 2(c), when the grating separation distance of the YbFO was set to be 11, 16, 20 and 29 mm, the net cavity dispersion was 0.074, 0.006, -0.048 and -0.170 ps², respectively. For different values of net cavity dispersion, pump thresholds for mode-locking and output powers are different, as shown in Fig. 2(d). The mode-locking pump thresholds for above four cases are 405, 95, 100 and 106 mW, corresponding to the output power of 5.0, 1.4, 2.3 and 2.4 mW, respectively. The pump power for the normal dispersion (0.074 ps²) regime is obvious higher than other cases.

Figures 3(a)-(d) show the four typical output spectra directly from the oscillator. The 0.17-nm narrow spectral bandwidth as well as high pump, high output power is the typical characteristic for dissipative soliton mode-locking in the normal dispersion regime, which was also observed in a dispersion managed Er-doped fiber laser with NALM scheme [37]. Successive increase of the grating separation led to a shift into near-zero net dispersion. In this regime, laser pulse experienced periodic stretch and compress while traversing the cavity [38]. As one of the distinct characteristics in the stretched pulse regime, its spectrum exhibits the widest bandwidth of

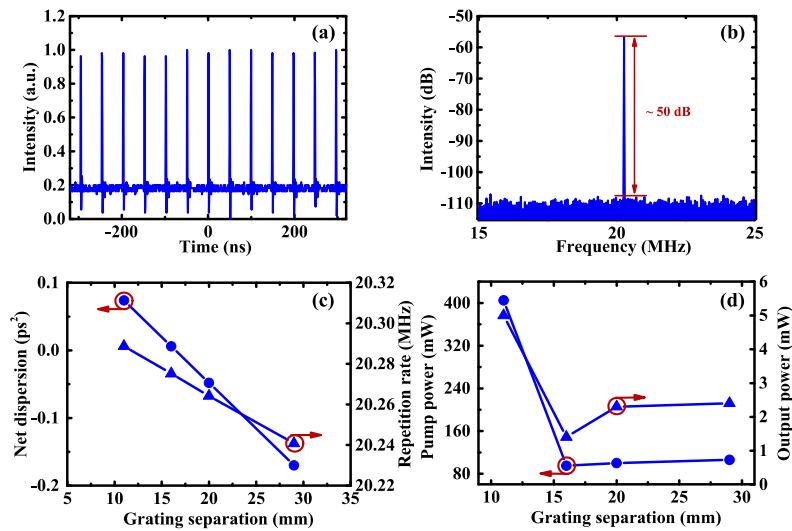


Fig. 2. (a) Output pulse trains measured by oscilloscope; (b) RF spectrum of output pulses with a resolution bandwidth of 3.3 kHz; (c) Net cavity dispersion and repetition rate as a function of the grating separation; (d) Pump power and output power as a function of the grating separation.

18 nm, as shown in Fig. 3(b). Further increase of grating separation moved the mode-locking state from stretched pulse regime to anomalous dispersion soliton regime. As a result, the spectral bandwidth reduced to 9.2 and 3.5 nm with net cavity dispersion of -0.048 and -0.170 ps², respectively.

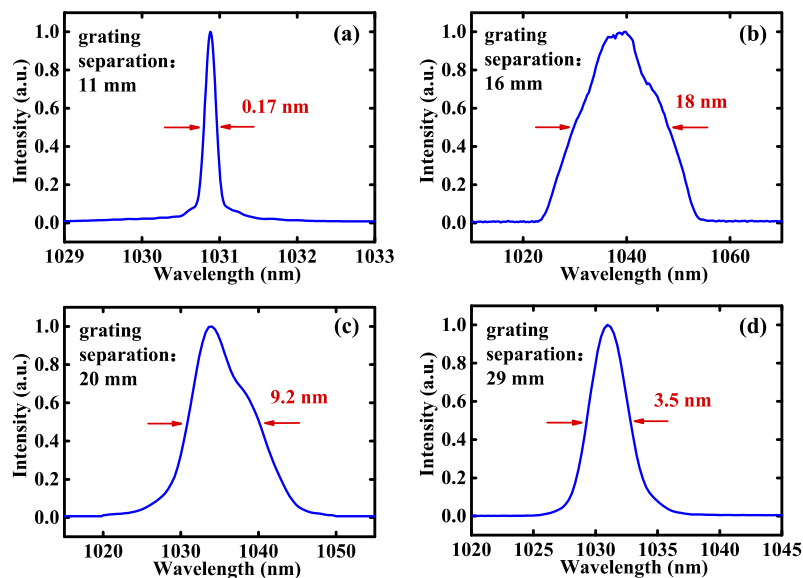


Fig. 3. Four typical output spectra of oscillator at different grating separations. (a) Normal dispersion regime; (b) Near-zero dispersion regime; (c) Negative dispersion of -0.048 ps²; (d) Negative dispersion of -0.170 ps².

The output power directly from the oscillator was only several milliwatts, which was not enough for conducting autocorrelation measurement in our lab. However, we could roughly estimate the pulse width by their spectral bandwidth. The Fourier-transform limited pulse durations for Gaussian shape pulse were calculated to be 9180, 86, 170 and 446 fs considering the measured spectral bandwidth of 0.17, 18, 9.2, and 3.5 nm.

3.2. Spectral broadening of the nonlinear fiber amplifier seeded by various solitons

Once stable mode-locking operation was obtained, we investigated the output spectra from the core-pumped single-clad nonlinear fiber amplifier for different values of net cavity dispersion from positive to negative values. We used optical spectrometer (AQ6370C, Yokogawa) to record the spectral evolution of amplified pulses with increased output power from 50 to 410 mW in logarithmic coordinates.

The spectral evolution for various input spectra are quite different. As shown in Fig. 4(a), output spectrum of dissipative soliton at the maximum power level of 410 mW almost had the same bandwidth as the seed. This is because nonlinear effects such as self-phase modulation (SPM) are balanced by the gain narrowing effect. We can also see that the spectral range of amplified spontaneous emission (ASE) was enlarged with the increased pump. However, their intensity was 25 dB smaller than that in the central wavelength, which indicates enough noise suppression in the amplifier. For the dissipative soliton with narrow spectral bandwidth and large pulse duration, the nonlinear accumulation was weak. In this case, the core-pumped single-clad amplifier worked in the linear regime.

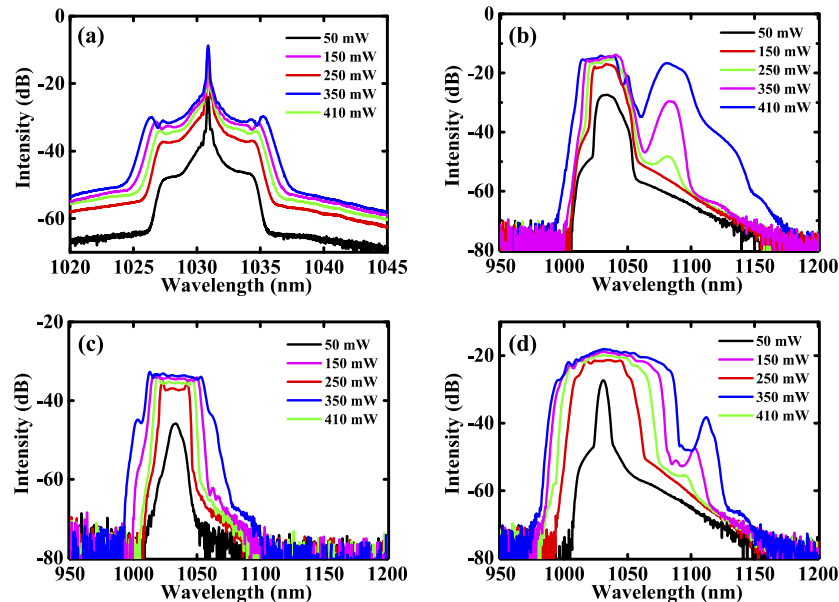


Fig. 4. Spectral evolution with increased output power for various input spectra: (a) Normal dispersion regime; (b) Near-zero dispersion regime; (c) Negative dispersion of -0.048 ps^2 ; (d) Negative dispersion of -0.170 ps^2 .

For stretched input pulses with broad spectral bandwidth, nonlinear effects are quite obvious in the core-pumped fiber amplifier. As shown in Fig. 4(b), SPM is the predominant effect for spectral broadening. As a result, the spectral bandwidth was enlarged from 18 to 30 nm. It should be noticed that a stimulated Raman spectral peak at 1080 nm is appeared and increased quickly with the pump power. Further increase the pump power might induce strong stimulated Raman

amplification and transfer the energy from original 1030 nm to Raman induced spectral band at 1080 nm.

As for the traditional soliton with moderate net cavity dispersion of -0.048 ps^2 , optical pulses experienced gradual spectral broadening due to SPM in the fiber amplifier, as shown in Fig. 4(c). The spectrum with symmetrical shape and steep edge is the typical characteristic of SPM enabled pulse spectral evolution. In this case, the spectral bandwidth was broadened from 9.2 to 44 nm.

When the net cavity dispersion was set to -0.170 ps^2 , obvious parabolic pulse evolution in the fiber amplifier was observed. The spectrum broadened rapidly due to the interplay between SPM and group-velocity dispersion. As shown in Fig. 4(d), a wide spectrum from 1012 to 1068 nm with 3-dB bandwidth of 56 nm was achieved, which is to our best of knowledge the widest spectrum generated from core-pumped single-clad fiber amplifier.

It is interesting that the broadest spectrum from the parabolic pulse evolution was obtained when the net cavity dispersion set to -0.170 ps^2 , corresponding to the narrowest input spectral bandwidth of 3.5 nm. We attribute this to the pulse width broadening caused by the fiber dispersion. Due to the accumulated normal dispersion of transmission fiber from output port of the oscillator to gain fiber (about 1.0 m in our case), the pulse width would inevitably broadened when propagating in optical fibers, which will greatly affect their spectral evolution in fiber amplifiers. Figure 5(a) shows the simulation results of pulse width evolution in a piece of SMF with length of 1.0 m using LaserFOAM software [39]. The input pulse was set to Fourier-transform limited Gaussian-shape pulse with spectral bandwidth of 18, 9.2, and 3.5 nm, respectively. The pulse chirp was set to zero for simplicity and fiber dispersion was set to $26 \text{ ps}^2/\text{km}$. It is quite clear that laser pulse with wider spectrum is temporally broadened to a much larger pulse duration. As a result, the smallest pulse width after propagating a piece of 1.0-m SMF is obtained with the narrowest spectral bandwidth of 3.5 nm. Figure 5(b) shows the simulation results of spectral bandwidth evolution of temporally broadened pulses mentioned above in a piece of gain fiber with 1.5-m length. In the simulation, fiber gain was set to 18 dB/m and nonlinear coefficient was set to $5 \text{ W}^{-1}\text{km}^{-1}$. The simulated spectral bandwidths after amplification for input pulse with spectral bandwidths of 18, 9.2, and 3.5 nm are 32, 45 and 57 nm, which are in good agreement with the experimental results of 30, 44 and 56 nm, respectively.

The logarithmic spectral broadening evolution for input pulse with 3.5-nm spectral bandwidth is shown in Fig. 5(c). With increased gain, the spectral shape gradually changed from rectangle to parabolic. The simulated result agreed well with the experimentally measured parabolic spectrum at maximum average power, as shown in Fig. 5(d). To verify the pulse re-compressibility of the broadest spectrum, we used a pair of gratings (1250 lines/mm) to build a compressor. Compressed pulses with an average power of 258 mW can be obtained, corresponding to the maximum compression efficiency of 63%. The measured autocorrelation trace was shown in the insert of Fig. 5(d), suggesting a de-convolved pulse width of 80 fs, which was larger than twice of the transform-limited pulse width due to uncompensated high-order dispersion and excessive nonlinearity caused by fiber sections before and after gain fiber. Although a low-intensity pedestal is observed, over 83% of the energy still lies within the main peak. Besides the dispersion of transmission fiber, we believe initial chirp value of the pulse also has an inevitable effect on the spectral evolution. According to the previous research, a chirp free pulse would experience faster spectral broadening than pulse with positive chirp in normal dispersive fiber amplifier [22].

Compared to the existing spectral broadening methods such as direct amplification, parabolic pre-shaping and pre-chirp managed amplification. Our proposed pre-chirp free method can be regarded as a balanced spectral broadening method with a simple structure and controllable parameters. Although direct amplification has the simplest structure which only contains an oscillator and an amplifier, the parameters of seed pulse and gain fiber should be well designed to achieve efficient parabolic amplification, let alone its high power femtosecond seed ($<200 \text{ fs}$, $\sim 200 \text{ mW}$) and free space coupling [24,25]. Pre-shaping or pre-chirp managed amplification

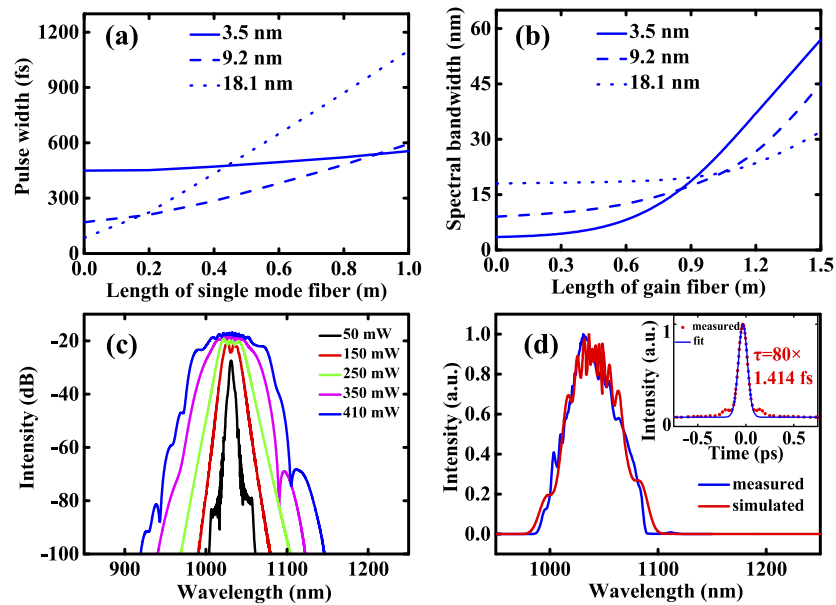


Fig. 5. (a) Simulated pulse width evolution in 1.0-m single mode fiber for transform limited Gaussian pulse; (b) Simulated spectral bandwidth change in 1.5-m gain fiber for temporally broadened pulse; (c) Simulated spectral evolution for input pulse of 3.5-nm bandwidth with increased average power; (d) Simulated and measured spectra of amplified parabolic pulse at 410 mW. The insert shows corresponding compressed pulse width of 80 fs.

adopts a more complex structure with an add-on module consisting of passive fiber or grating pairs before amplifier to lower the requirement of laser oscillator and improve the re-compressed pulse quality [26,31]. Our pre-chirper free method controls pulse spectral evolution by manipulating the dispersion of laser oscillator. The structure is as simple as direct amplification, but the freedom to manipulate parameters of seed pulse is to some extent similar to pre-shaping or pre-chirp managed amplification. The remaining drawback of our method is that the adjustable range and accuracy of oscillator's parameter is still limited by its mode-locking operation range. As for the newly developed amplification with gain-managed nonlinearity, it can obtain amplified pulse with spectrum beyond gain-narrowing limit and compressible pulse width less than 50 fs [16,28]. However, the input seed wavelength should be well-chosen to match the dynamically evolving gain spectrum and gain fiber should be long, highly doped fiber to allow continuous pulse evolution from similarity to gain-managed nonlinearity, which adding additional requirement for designing of an amplifier.

Currently, we used subsequent optical filter and two additional core-pumped fiber amplifiers after spectral broadening for multi-color CARS. This filtered-in-the-middle, all core-pumped fiber laser system has three advantages in biomedical imaging requiring tunable picosecond laser compared to filtered-at-the-terminal double-clad fiber amplifier. First, the output power from the core-pumped laser (typically <1 W) is enough for exciting most of biomedical samples, thus lower power consumption can be achieved [29]. Second, high-speed wavelength tuning can be easily achieved in filtered-in-the-middle, core-pumped fiber laser system due to the low damage threshold of commercially-available fast tunable filters [7]. Third, core-pumped fiber amplifier is generally easier for all-fiber integration than double-clad fiber amplifier.

3.3. Coherent anti-Stokes Raman imaging

Next, we will turn to CARS imaging by using the synchronized tunable pulses. For simplicity, we denoted laser pulses around 1 μm as the Stokes light and pulses centered at 790 nm as the Pump light. The spectral broadened pulses from the nonlinear parabolic amplifier were used as the seed for tuning the wavelength of Stokes light. Synchronization between Stokes and Pump light was achieved by injecting 30-mW 1030-nm pulses into Er-doped laser oscillator, resulting a cavity mismatch distance of 150 μm , which was long enough to maintain stable synchronization status for CARS imaging. Wavelength tunable range of 60 nm with bandwidth of 0.8 nm was achieved by a commercial optical filter. After further amplification, output power at 1030 nm reached to around 200 mW with spectral bandwidth of 1.44 nm. The corresponding pulse width was measured to be 3.2 ps. For other wavelengths, output power of >100 mW can be obtained. The Pump pulses had an average power of 68 mW. They had a spectral bandwidth of 0.22 nm and pulse duration of 24 ps.

Precise temporal and spatial overlap of synchronized dual-color pulses were achieved by a free-space optical delay line and a dichroic mirror. Then the laser pulses were sent to a commercial inverted laser scanning microscope (Olympus, FV1200) for nonlinear biomedical imaging of mouse ear. The image acquisition rate was 2 $\mu\text{s}/\text{pixel}$ and the imaging size was 512 \times 512. Due to the redundant time in the experiment, the time required to obtain an image was 1.08 s. We used objective with numerical aperture of 1.2 for focusing. The average power for Pump and Stokes laser on the sample was approximately 20 and 10 mW, respectively. For detection, a short pass filter (700 nm) and a bandpass filter (640 \pm 20 nm) were used to eliminate the background light. After that, CARS signal was collected by a photo multiplier tube (PMT). Figures 6(a) and 6(b) show the CARS images of lipid and protein distribution measured at Raman bands of 2850 and 2930 cm^{-1} . By replacing the bandpass filter before the PMT, the microscope

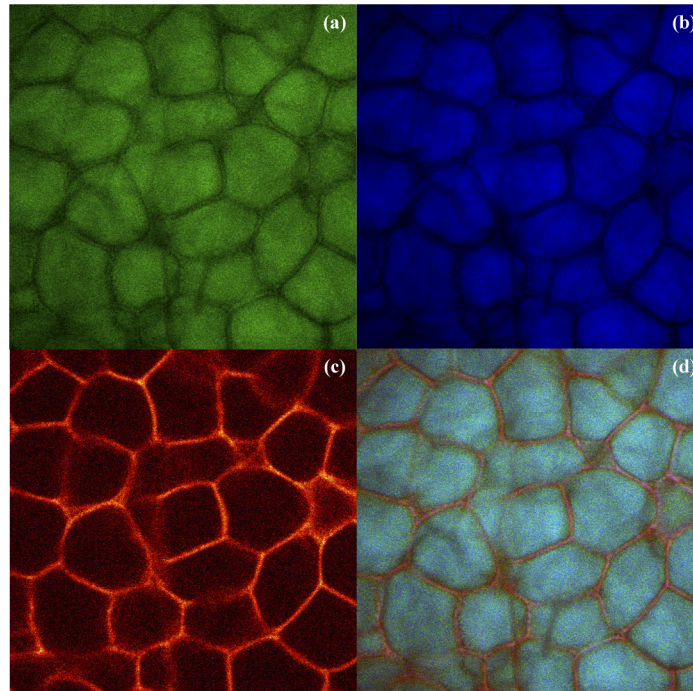


Fig. 6. CARS images of fresh mouse ear tissue at (a) 2850 cm^{-1} and (b) 2930 cm^{-1} ; (c) SHG image of fresh mouse ear tissue; (d) Combined image of CARS and SHG.

can be switched to SHG mode. As shown in Fig. 6(c), the collagen distribution can be clearly seen. By combining both CARS and SHG images, a composite multi-mode nonlinear image can be obtained, as shown in Fig. 6(d).

4. Conclusion

In conclusion, we have realized tunable dual-color pulses from passively synchronized Er- and Yb-doped fiber lasers. The involved spectral evolution in a core-pumped single-mode fiber amplifier has been systematically investigated with the seeds of dissipative soliton, stretched pulse and soliton. It has been found that the net cavity dispersion in the oscillator would impose a significant impact on the spectro-temporal characteristic for the amplified pulses. In the experiment, a broadband parabolic spectrum with 56-nm bandwidth was optimized at a net cavity dispersion about -0.170 ps^2 . By using the input pulse with a narrow spectral bandwidth, parabolic pulse evolution occurred in the nonlinear fiber amplifier. These findings may be useful to design a fiber amplifier for generating broadband spectrum without the need of a pre-chirper. Based on the achieved broadband spectrum, the wavelength of Yb-doped fiber laser can be continuously tuned to match Raman bands of 2850 and 2930 cm^{-1} in combining with the frequency doubled Er-doped laser at 790 nm. The implemented tunable synchronized dual-color pulses with an all-polarization-maintaining fiber design would promote the nonlinear biomedical imaging into subsequent clinical applications.

Funding. National Natural Science Foundation of China (11974248, 62175064, 81671725, 61975033, 11727812); Shanghai Municipal Science and Technology Major Project (2018SHZDZX01, 2017SHZDZX01); ZJLab.

Disclosures. The authors declare no conflicts of interest.

Data availability. Data is available upon reasonable request.

References

1. J. X. Cheng and X. S. Xie, "Vibrational spectroscopic imaging of living systems: An emerging platform for biology and medicine," *Science* **350**(6264), aaa8870 (2015).
2. L. Wei, Z. Chen, L. Shi, R. Long, A. V. Anzalone, L. Zhang, F. Hu, R. Yuste, V. W. Cornish, and W. Min, "Super-multiplex vibrational imaging," *Nature* **544**(7651), 465–470 (2017).
3. A. H. Hill, B. Manifold, and D. Fu, "Tissue imaging depth limit of stimulated Raman scattering microscopy," *Biomed. Opt. Express* **11**(2), 762–774 (2020).
4. M. Ji, S. Lewis, S. Camelo-Piragua, S. H. Ramkissoon, M. Snuderl, S. Venneti, A. Fisher-Hubbard, M. Garrard, D. Fu, and A. C. Wang, "Detection of human brain tumor infiltration with quantitative stimulated Raman scattering microscopy," *Sci. Transl. Med.* **7**(309), 309ra163 (2015).
5. M. Ji, M. Arbel, L. Zhang, C. W. Freudiger, S. S. Hou, D. Lin, X. Yang, B. J. Bacskai, and X. S. Xie, "Label-free imaging of amyloid plaques in Alzheimer's disease with stimulated Raman scattering microscopy," *Sci. Adv.* **4**(11), eaat7715 (2018).
6. E. Pshenay-Severin, H. Bae, K. Reichwald, G. Matz, J. Bierlich, J. Kobelke, A. Lorenz, A. Schwuchow, T. Meyer-Zedler, M. Schmitt, B. Messerschmidt, and J. Popp, "Multimodal nonlinear endomicroscopic imaging probe using a double-core double-clad fiber and focus-combining micro-optical concept," *Light: Sci. Appl.* **10**(1), 207 (2021).
7. Y. Suzuki, K. Kobayashi, Y. Wakisaka, D. Deng, S. Tanaka, C. Huang, C. Lei, C. Sun, H. Liu, Y. Fujiwaki, S. Lee, A. Isozaki, Y. Kasai, T. Hayakawa, S. Sakuma, F. Arai, K. Koizumi, H. Tezuka, M. Inaba, K. Hiraki, T. Ito, M. Hase, S. Matsusaka, K. Shiba, K. Suga, M. Nishikawa, M. Jona, Y. Yatomi, Y. Yalikun, Y. Tanaka, T. Sugimura, N. Nitta, K. Goda, and Y. Ozeki, "Label-free chemical imaging flow cytometry by high-speed multicolor stimulated Raman scattering," *P. Natl. Acad. Sci. USA* **116**(32), 15842–15848 (2019).
8. B. Zhang, H. Xu, J. Chen, X. Zhu, Y. Xue, Y. Yang, J. Ao, Y. Hua, and M. Ji, "Highly specific and label-free histological identification of microcrystals in fresh human gout tissues with stimulated Raman scattering," *Theranostics* **11**(7), 3074–3088 (2021).
9. J. Ao, X. Fang, X. Miao, J. Ling, H. Kang, S. Park, C. Wu, and M. Ji, "Switchable stimulated Raman scattering microscopy with photochromic vibrational probes," *Nat. Commun.* **12**(1), 3089 (2021).
10. T. Gottschall, T. Meyer, M. Schmitt, J. Popp, J. Limpert, and A. Tünnermann, "Advances in laser concepts for multiplex, coherent Raman scattering micro-spectroscopy and imaging," *TrAC, Trends Anal. Chem.* **102**, 103–109 (2018).
11. K. Yang, P. Ye, S. Zheng, J. Jiang, K. Huang, Q. Hao, and H. Zeng, "Polarization switch of four-wave mixing in a tunable fiber optical parametric oscillator," *Opt. Express* **26**(3), 2995–3003 (2018).
12. K. Yang, S. Zheng, P. Ye, Q. Hao, K. Huang, and H. Zeng, "Fiber-based optical parametric oscillator with flexible repetition rates by rational harmonic pumping," *Opt. Express* **27**(4), 4897–4906 (2019).

13. T. Gottschall, T. Meyer Zedler, M. Schmitt, R. Huber, J. Popp, A. Tünnermann, and J. Limpert, "Ultra-compact tunable fiber laser for coherent anti-Stokes Raman imaging," *J. Raman Spectrosc.* **52**(9), 1561–1568 (2021).
14. K. Yang, L. Huo, J. Ao, Q. Wang, Q. Hao, M. Yan, K. Huang, M. Ji, and H. Zeng, "Fast tunable all-polarization-maintaining supercontinuum fiber laser for CARS microscopy," *Appl. Phys. Express* **14**(6), 062004 (2021).
15. Y. Zhang, J. Jiang, K. Liu, S. Wang, Z. Ma, W. Chen, and T. Liu, "Dual-Frequency CARS Excitation Source With Two Independent-Tunable Stokes Wavelengths Using PM-PCF and Vector Adjustment," *J. Lightwave Technol.* **38**(8), 2392–2399 (2020).
16. P. Sidorenko, W. Fu, and F. Wise, "Nonlinear ultrafast fiber amplifiers beyond the gain-narrowing limit," *Optica* **6**(10), 1328–1333 (2019).
17. J. M. Dudley, G. E. Genty, and S. E. Coen, "Supercontinuum generation in photonic crystal fiber," *Rev. Mod. Phys.* **78**(4), 1135–1184 (2006).
18. Y. Shen, A. A. Voronin, A. M. Zheltikov, S. P. O Connor, V. V. Yakovlev, A. V. Sokolov, and M. O. Scully, "Picosecond supercontinuum generation in large mode area photonic crystal fibers for coherent anti-Stokes Raman scattering microspectroscopy," *Sci. Rep.* **8**(1), 9526 (2018).
19. K. Yang, Y. Shen, J. Ao, S. Zheng, Q. Hao, K. Huang, M. Ji, and H. Zeng, "Passively synchronized mode-locked fiber lasers for coherent anti-Stokes Raman imaging," *Opt. Express* **28**(9), 13721–13730 (2020).
20. A. M. Heidt, J. S. Feehan, J. H. V. Price, and T. Feurer, "Limits of coherent supercontinuum generation in normal dispersion fibers," *J. Opt. Soc. Am. B* **34**(4), 764–775 (2017).
21. B. Figueroa, W. Fu, T. Nguyen, K. Shin, B. Manifold, F. Wise, and D. Fu, "Broadband hyperspectral stimulated Raman scattering microscopy with a parabolic fiber amplifier source," *Biomed. Opt. Express* **9**(12), 6116–6131 (2018).
22. C. Finot, F. Parmigiani, P. Petropoulos, and D. Richardson, "Parabolic pulse evolution in normally dispersive fiber amplifiers preceding the similariton formation regime," *Opt. Express* **14**(8), 3161–3170 (2006).
23. H. Song, B. Liu, W. Chen, Y. Li, Y. Song, S. Wang, L. Chai, C. Wang, and M. Hu, "Femtosecond laser pulse generation with self-similar amplification of picosecond laser pulses," *Opt. Express* **26**(20), 26411–26421 (2018).
24. D. N. Papadopoulos, Y. Zaouter, M. Hanna, F. Druon, and P. Georges, "Generation of 63 fs 4.1 MW peak power pulses from a parabolic fiber amplifier operated beyond the gain bandwidth limit," *Opt. Lett.* **32**(17), 2520–2522 (2007).
25. Y. Deng, C. Chien, B. G. Fidric, and J. D. Kafka, "Generation of sub-50 fs pulses from a high-power Yb-doped fiber amplifier," *Opt. Lett.* **34**(22), 3469–3471 (2009).
26. F. Walter, T. Yuxing, T. S. McComb, T. L. Lowder, and F. W. Wise, "Limits of femtosecond fiber amplification by parabolic pre-shaping," *J. Opt. Soc. Am. B* **34**(3), A37–A42 (2017).
27. Y. Liu, C. Wang, D. Luo, C. Yang, J. Li, L. Ge, Y. Pan, and W. Li, "Generation of 70 fs broadband pulses in a hybrid nonlinear amplification system with mode-locked Yb:YAG ceramic oscillator," *J. Opt. (Bristol, U. K.)* **19**(12), 125501 (2017).
28. P. Sidorenko and F. Wise, "Generation of 1 μ J and 40 fs pulses from a large mode area gain-managed nonlinear amplifier," *Opt. Lett.* **45**(14), 4084–4087 (2020).
29. Y. Fu, H. Wang, R. Shi, and J. X. Cheng, "Characterization of photodamage in coherent anti-Stokes Raman scattering microscopy," *Opt. Express* **14**(9), 3942–3951 (2006).
30. T. Gottschall, T. Meyer, M. Baumgartl, C. Jauregui, M. Schmitt, J. Popp, J. Limpert, and A. Tünnermann, "Fiber-based light sources for biomedical applications of coherent anti-Stokes Raman scattering microscopy," *Laser Photon. Rev.* **9**(5), 435–451 (2015).
31. H. W. Chen, J. Lim, S. W. Huang, D. N. Schimpf, and G. Chang, "Optimization of femtosecond Yb-doped fiber amplifiers for high-quality pulse compression," *Opt. Express* **20**(27), 28672–28682 (2012).
32. X. Gu, X. Cao, Y. Li, H. Chen, and Y. Liu, "Nonlinear pulse compression of an all-normal-dispersion Yb-fiber laser by a single-mode fiber amplifier," *Opt. Eng.* **59**(10), 106105 (2020).
33. Y. Hua, G. Chang, F. X. Kärtner, and D. N. Schimpf, "Pre-chirp managed, core-pumped nonlinear PM fiber amplifier delivering sub-100-fs and high energy (10 nJ) pulses with low noise," *Opt. Express* **26**(5), 6427–6438 (2018).
34. Y. Ozeki, T. Asai, J. Shou, and H. Yoshimi, "Multicolor Stimulated Raman Scattering Microscopy With Fast Wavelength-Tunable Yb Fiber Laser," *IEEE J. Sel. Top. Quant.* **25**(1), 1–11 (2019).
35. C. Kong, C. Pilger, H. Hachmeister, X. Wei, T. H. Cheung, C. S. W. Lai, N. P. Lee, K. K. Tsia, K. K. Y. Wong, and T. Huser, "High-contrast, fast chemical imaging by coherent Raman scattering using a self-synchronized two-colour fibre laser," *Light: Sci. Appl.* **9**(1), 25 (2020).
36. T. Yu, J. Fang, Q. Hao, K. Yang, M. Yan, K. Huang, and H. Zeng, "High-precision passive stabilization of repetition rate for a mode-locked fiber laser based on optical pulse injection," *Opt. Express* **29**(13), 20930–20940 (2021).
37. Z. Łaszczysz and G. Soboń, "Dispersion management of a nonlinear amplifying loop mirror-based erbium-doped fiber laser," *Opt. Express* **29**(2), 2690–2702 (2021).
38. A. S. Mayer, W. Grosinger, J. Fellingner, G. Winkler, L. W. Perner, S. Droste, S. H. Salman, C. Li, C. M. Heyl, I. Hartl, and O. H. Heckl, "Flexible all-PM NALM Yb-fiber laser design for frequency comb applications: operation regimes and their noise properties," *Opt. Express* **28**(13), 18946–18968 (2020).
39. A. A. Amorim, M. V. Tognetti, P. Oliveira, J. L. Silva, L. M. Bernardo, F. X. Kartner, and H. M. Crespo, "Sub-two-cycle pulses by soliton self-compression in highly nonlinear photonic crystal fibers," *Opt. Lett.* **34**(24), 3851–3853 (2009).